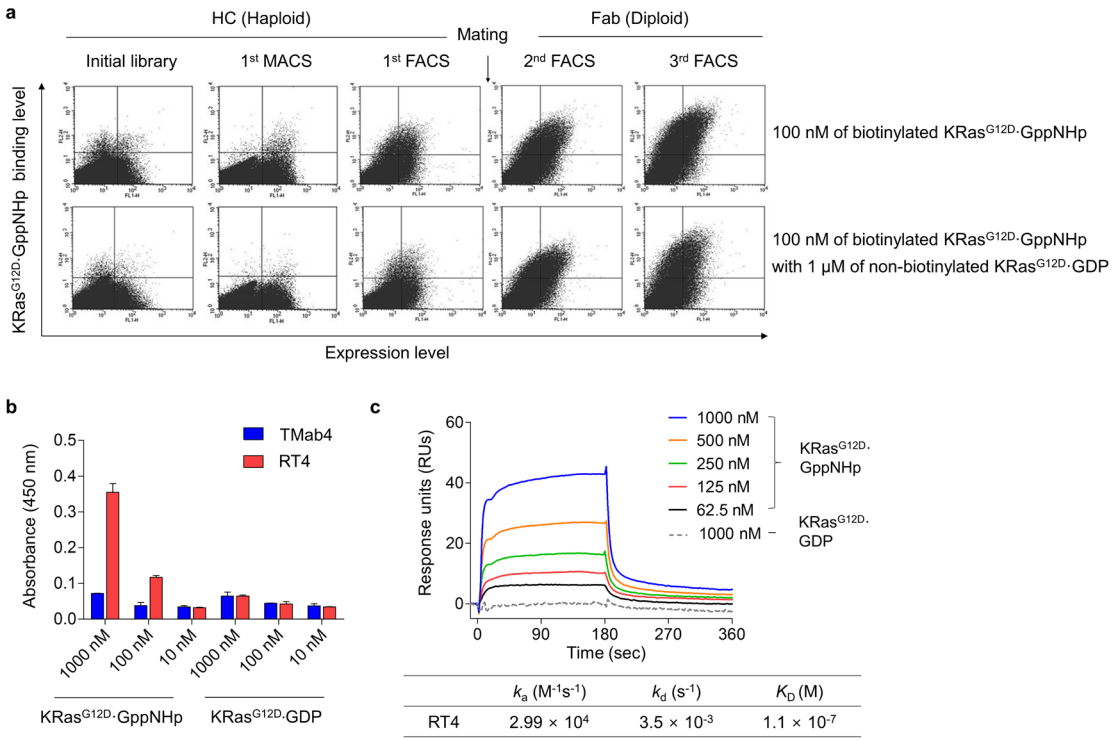


**Supplementary Figure 1 Isolation and characterization of GppNHp-bound active KRas$^{G12D}$-specific binding RT4.** (**a**) Flow cytometric analysis of antigen binding and expression levels of HC in the haploid library and Fab in the mated diploid yeast library. (**b**) Binding activity of RT4 and TMab4 with KRas$^{G12D}$·GppNHp and KRas$^{G12D}$·GDP, determined by direct ELISA. ELISA plates were coated with 5 μg ml$^{-1}$ of antibodies and then incubated with the antigen at concentrations of 10, 100, and 1000 nM. Error bars represent the mean ± s.d. ($n$ = 3). (**c**) Representative SPR sensorgrams showing the kinetic interactions of RT4 with KRas$^{G12D}$·GppNHp. The injection of KRas$^{G12D}$·GDP (1 μM) (dashed line) exhibited negligible binding to RT4. The inset table shows the kinetic interaction parameters.

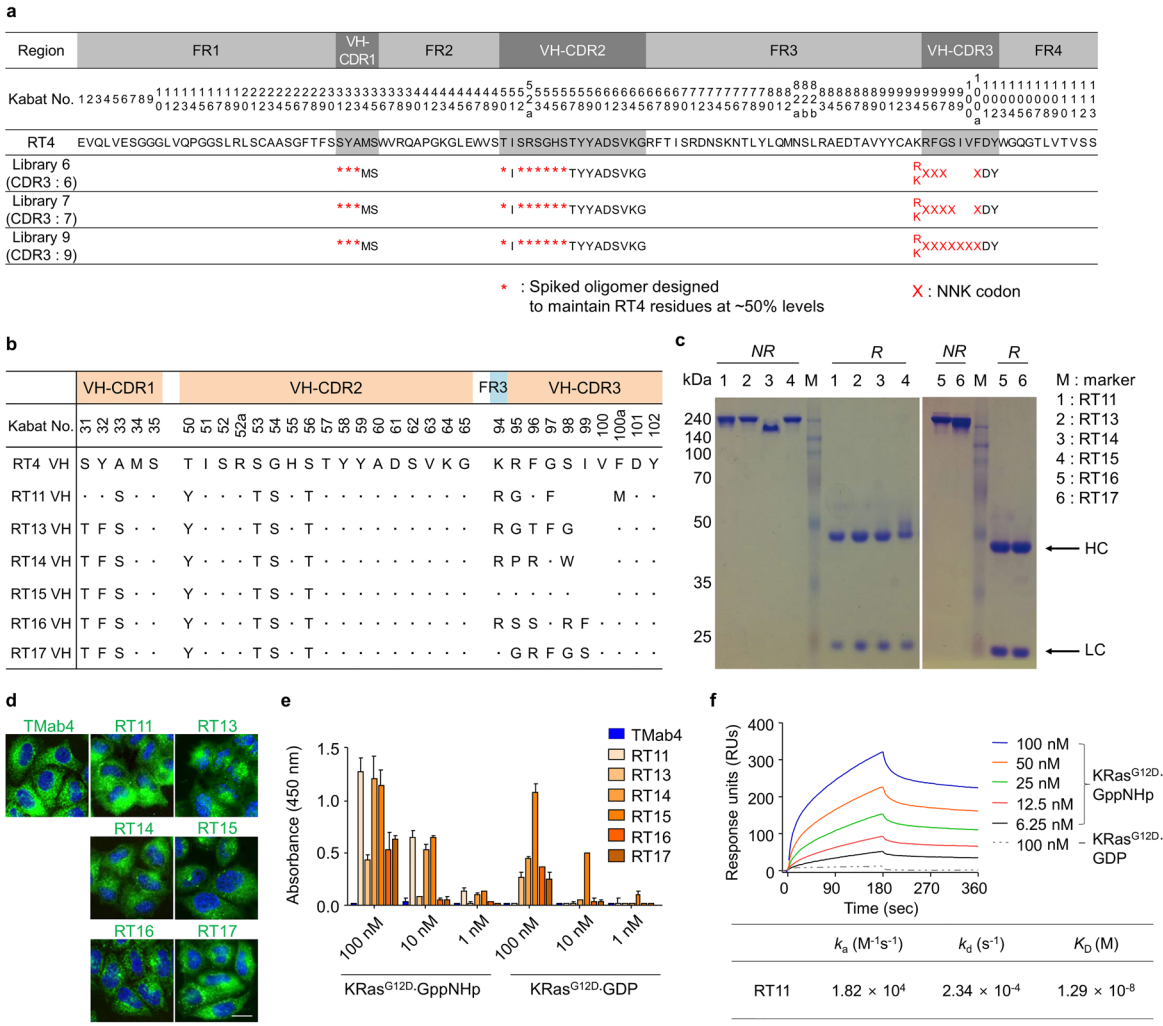
a
Region
FR1
VH-CDR1
FR2
VH-CDR2
FR3
VH-CDR3
FR4
Kabat No.
RT4 EVQLVESGGGLVQPGGSLRLSCAASGFTFSSYAMSWVRQAPGKGLEWVSTISRSGHSTYYADSVKGRFTISRDNSKNTLYLQMNSLRAEDTAVYYCAKRFGSIVFDYWGQGTLVTVSS
Library 6 (CDR3 : 6)
Library 7 (CDR3 : 7)
Library 9 (CDR3 : 9)
* : Spiked oligomer designed to maintain RT4 residues at ~50% levels
X : NNK codon
b
VH-CDR1
VH-CDR2
FR3
VH-CDR3
Kabat No.
RT4 VH S Y A M S T I S R S G H S T Y Y A D S V K G K R F G S I V F D Y
RT11 VH
RT13 VH
RT14 VH
RT15 VH
RT16 VH
RT17 VH
c
NR
R
NR
R
kDa 1 2 3 4 M 1 2 3 4 5 6 M 5 6
240
140
100
70
50
35
25
HC
LC
M : marker
1 : RT11
2 : RT13
3 : RT14
4 : RT15
5 : RT16
6 : RT17
d
TMab4
RT11
RT13
RT14
RT15
RT16
RT17
e
Absorbance (450 nm)
1.5
1.0
0.5
0.0
TMab4
RT11
RT13
RT14
RT15
RT16
RT17
100 nM
10 nM
1 nM
100 nM
10 nM
1 nM
KRasG12D.GppNHp
KRasG12D.GDP
f
Response units (RUs)
400
300
200
100
0
0
90
180
270
360
Time (sec)
100 nM
50 nM
25 nM
12.5 nM
6.25 nM
100 nM
KRasG12D. GppNHp
KRasG12D. GDP
ka (M-1s-1)
kd (s-1)
KD (M)
RT11 1.82 × 10^4 2.34 × 10^-4 1.29 × 10^-8

**Supplementary Figure 2 Affinity maturation of RT4 and biochemical characterization of the isolated RT4 variants.** (**a**) Library construction scheme. Amino acid sequence alignment of RT4 VH showing the positions of conserved and mutated residues in the three libraries differing in the length of VH-CDR3, dubbed library 6, 7, and 9. The residues (31–33 residues) of VH-CDR1 and (50, 52–56 residues) of VH-CDR2, highlighted by asterisks (*), were randomly mutated, while maintaining the original amino acids at each residue of RT4 at a frequency of ~50%, using designed oligonucleotides. The VH-CDR3 region (residues 95–100a) was randomized with the degenerated codon of NNK, as indicated by 'X', which resulted in variation in the total length of 6, 7, and 9 residues. The framework residue of 94 was also permutated with degenerate codons of ARG to introduce Arg or Lys, in an attempt to cover the most conserved amino acids at the residues in human antibodies. Numbering is according to the Kabat definition. (**b**) Amino acid sequence alignment of the isolated RT4 variants. (**c**) Reducing ('*R*') and non-reducing ('*NR*') SDS-PAGE analyses of the purified RT4 variants (each 5 μg) in the human IgG1 format. (**d**) Cellular internalization and cytosolic localization of the purified TMab4 (green) and RT4 variants (green) in HeLa cells treated with antibodies (1 μM) for 6 h at 37 °C and then analyzed by confocal microscopy. Nuclei were counterstained with Hoechst 33342 (blue). Scale bar, 20 μm. (**e**) Binding specificity of RT4 variants to $KRas^{G12D}$·GppNHp or $KRas^{G12D}$·GDP, determined by direct ELISA. ELISA plates were coated with 5 μg $ml^{-1}$ of antibodies and then incubated with the antigen at concentrations of 1, 10, and 100 nM. Error bars represent the mean ± s.d. ($n$ = 3). (**f**) Representative SPR sensorgrams showing the kinetic interactions of RT11 with $KRas^{G12D}$·GppNHp. The injection of $KRas^{G12D}$·GDP (1 μM) (dashed line) exhibited negligible binding to RT11. The inset table shows the kinetic interaction parameters.

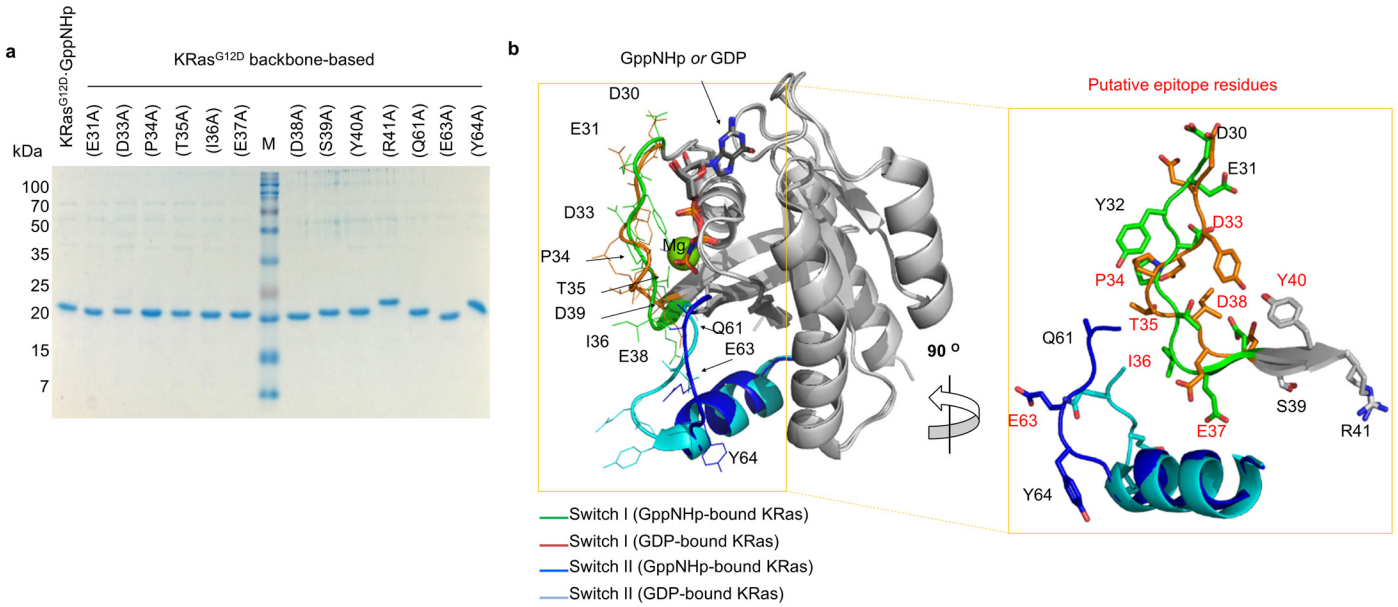


**Supplementary Figure 3 Epitope mapping of RT11 iMab by alanine-scanning mutagenesis.** (**a**) Reducing SDS-PAGE analyses of bacterially expressed and purified KRas$^{G12D}$ mutants (residue 1–168) with Ala mutation at the indicated residues. (**b**) Highlight of the epitopes of RT11 (red in the right panel) on the three-dimensional structure of KRas, determined by alanine scanning mutagenesis as shown in Fig. 1e. Three-dimensional structural comparison between GDP-bound inactive KRas (PDB ID: 4EPV)[1] and GppNHp-bound active KRas (PDB ID: 3GFT) shows conformational differences only in the switch I and II regions. Both GppNHp and GDP are shown as sticks colored according to heteroatoms (oxygen: red; nitrogen: blue; carbon: gray; phosphorus: orange), and the $Mg^{2+}$ ion is shown as a green sphere. The switch I and switch II regions of KRas·GppNHp and KRas·GDP are represented by green/blue or orange/cyan wires, respectively, with Ala mutation residues indicated. The rest of the protein structure is displayed in gray ribbon. The images were generated using PyMol program (Schrödinger).

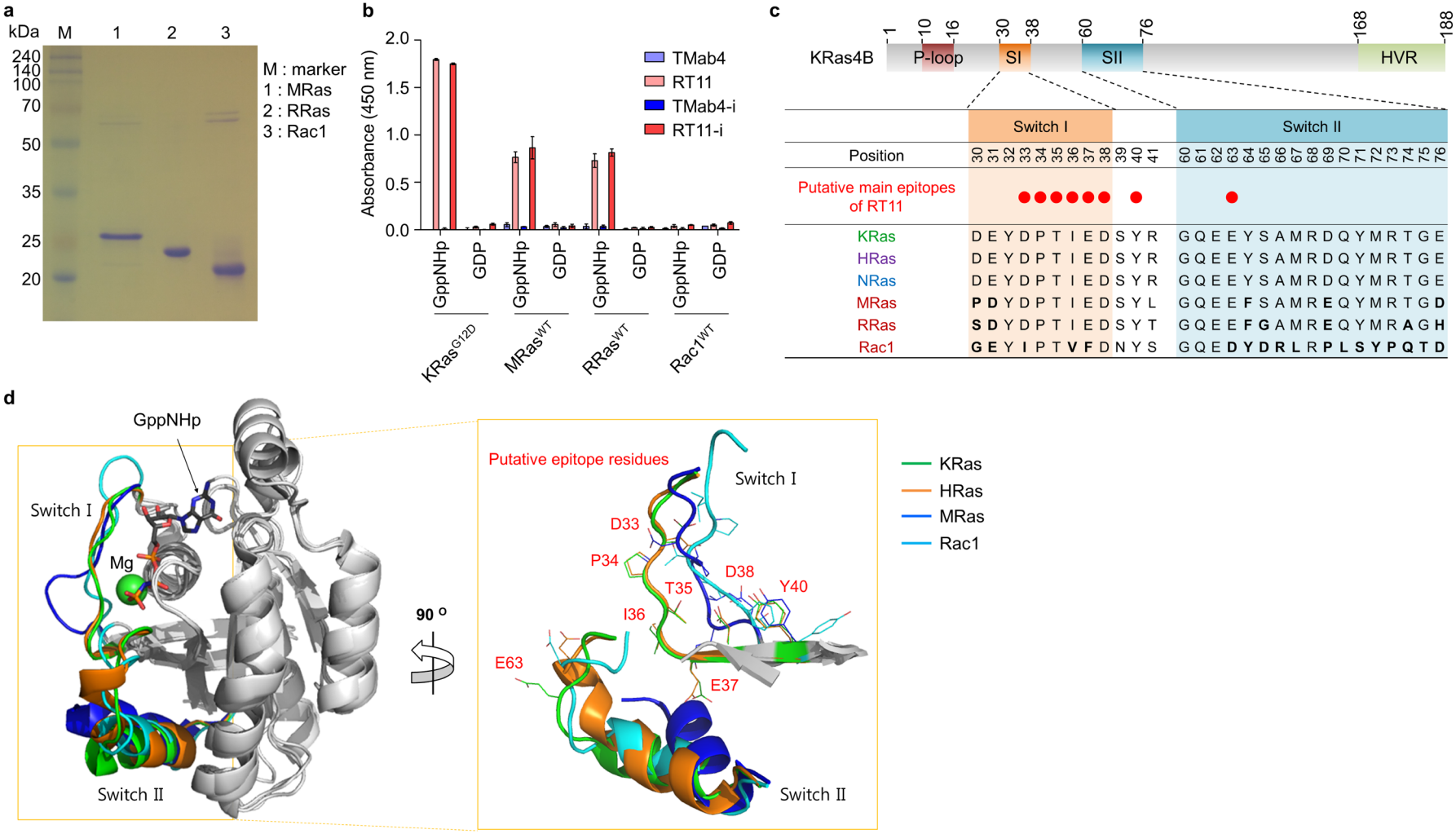
a
kDa
M
1
2
3
240
140
100
70
50
35
25
20
M : marker
1 : MRas
2 : RRas
3 : Rac1
b
Absorbance (450 nm)
2.0
1.5
1.0
0.5
0.0
TMab4
RT11
TMab4-i
RT11-i
GppNHp
GDP
KRasG12D
MRasWT
RRasWT
Rac1WT
c
KRas4B
P-loop
SI
SII
HVR
Switch I
Switch II
Position
Putative main epitopes of RT11
KRas D E Y D P T I E D S Y R G Q E E Y S A M R D Q Y M R T G E
HRas D E Y D P T I E D S Y R G Q E E Y S A M R D Q Y M R T G E
NRas D E Y D P T I E D S Y R G Q E E Y S A M R D Q Y M R T G E
MRas P D Y D P T I E D S Y L G Q E E F S A M R E Q Y M R T G D
RRas S D Y D P T I E D S Y T G Q E E F G A M R E Q Y M R A G H
Rac1 G E Y I P T V F D N Y S G Q E D Y D R L R P L S Y P Q T D
d
GppNHp
Switch I
Mg
Switch II
90 °
Putative epitope residues
D33
P34
T35
I36
D38
Y40
E63
E37
KRas
HRas
MRas
Rac1

**Supplementary Figure 4 RT11/RT11-i binds weakly to the active forms of MRas and RRas, but does not cross-react with Rac1.** (**a**) Reducing SDS-PAGE analyses of bacterially expressed and purified $MRas^{WT}$, $RRas^{WT}$, and $Rac1^{WT}$. (**b**) Binding activity of the indicated antibodies to the GppNHp-bound active forms or GDP-bound inactive forms of $MRas^{WT}$, $RRas^{WT}$, and $Rac1^{WT}$, compared to that of active $KRas^{G12D}$. ELISA plates were coated with 5 μg $ml^{-1}$ of antibodies and then incubated with the antigen at 100 nM. Error bars represent the mean ± s.d. ($n$ = 3). (**c**) Comparison of KRas residues in the switch I and II regions with those of HRas and NRas as well as other Ras superfamily GTPases such as MRas, RRas, and Rac1. The residues identified as putative binding epitopes of RT11 on $KRas^{G12D}$ by alanine scanning mutagenesis are highlighted as red circles. The residue numbering is based on the sequence of KRas. (**d**) Comparison of the crystal structures of GppNHp-bound active KRas (PDB ID: 3GFT), HRas (PDB ID: 1CTQ)[2], MRas (PDB ID: 1X1S)[3], and Rac1 (PDB ID: 5FI0)[4], highlighting the putative binding epitopes of RT11 on KRas (right panel). The switch I and II regions of KRas superimpose well with HRas showing root-mean-square-deviations of 0.45Å, but poorly with MRas and Rac1 showing root-mean-square-deviations of 2.06 and 2.47 Å, respectively. The crystal structure of GppNHp-bound RRas has not yet been determined, but it is expected to be similar to that of MRas rather than to that of KRas based on primary sequence homology (60.9% and 51.8% sequence identity with MRas and KRas, respectively)[5,6]. The images were generated using the PyMol program (Schrödinger).

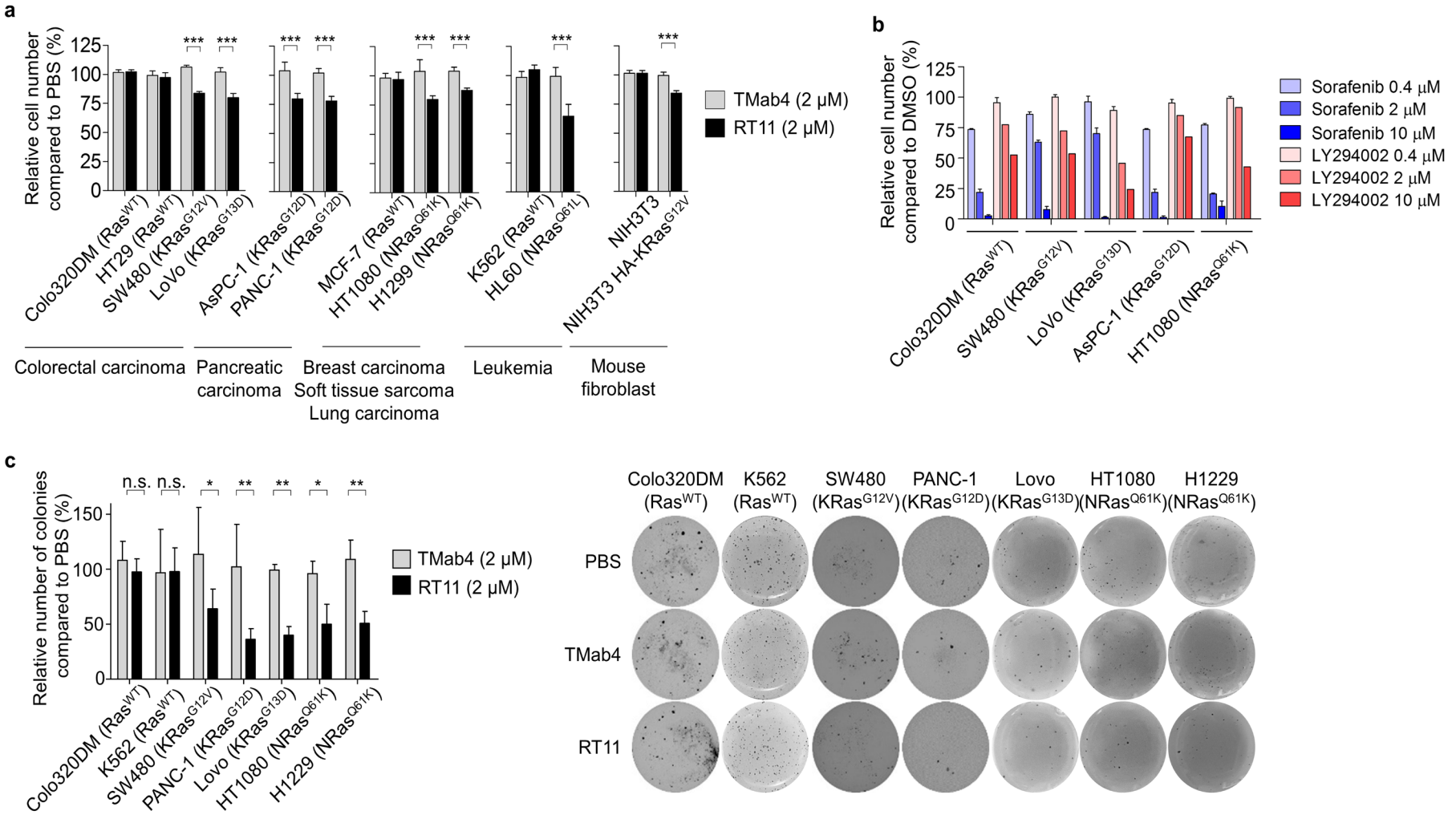
a
Relative cell number compared to PBS (%)
125
100
75
50
25
0
***
TMab4 (2 μM)
RT11 (2 μM)
Colo320DM (RasWT)
HT29 (RasWT)
SW480 (KRasG12V)
LoVo (KRasG13D)
AsPC-1 (KRasG12D)
PANC-1 (KRasG12D)
MCF-7 (RasWT)
HT1080 (NRasQ61K)
H1299 (NRasQ61K)
K562 (RasWT)
HL60 (NRasQ61L)
NIH3T3
NIH3T3 HA-KRasG12V
Colorectal carcinoma
Pancreatic carcinoma
Breast carcinoma
Soft tissue sarcoma
Lung carcinoma
Leukemia
Mouse fibroblast
b
Relative cell number compared to DMSO (%)
Sorafenib 0.4 μM
Sorafenib 2 μM
Sorafenib 10 μM
LY294002 0.4 μM
LY294002 2 μM
LY294002 10 μM
Colo320DM (RasWT)
SW480 (KRasG12V)
LoVo (KRasG13D)
AsPC-1 (KRasG12D)
HT1080 (NRasQ61K)
c
Relative number of colonies compared to PBS (%)
150
100
50
0
n.s.
*
**
TMab4 (2 μM)
RT11 (2 μM)
Colo320DM (RasWT)
K562 (RasWT)
SW480 (KRasG12V)
PANC-1 (KRasG12D)
Lovo (KRasG13D)
HT1080 (NRasQ61K)
H1229 (NRasQ61K)
PBS
TMab4
RT11

**Supplementary Figure 5 RT11 inhibits the growth of tumor cells harboring oncogenic Ras mutants, but not those with $Ras^{WT}$.** (**a, b**) Cellular proliferation assay in indicated cells, treated twice at 0 and 72 h with the indicated concentration of antibody (RT11 or TMab4) (**a**) or the pharmacological inhibitor (Raf kinase inhibitor sorafenib or PI3K-Akt inhibitor LY294002) (**b**) for 6 d. Error bars represent the mean ± s.d. ($n = 3$). $^{**}P < 0.01$, $^{***}P < 0.001$. (**c**) Inhibition of soft agar colony formation of tumor cells by RT11. Anchorage-independent cell growth was examined by soft agar colony formation assays using the oncogenic KRas mutant, NRas mutant, and $Ras^{WT}$ cells, treated with RT11 (2 μM) and TMab4 (2 μM) every 72 h for 2–3 weeks. Following treatment, the number of colonies (diameter > 200 μm) was counted after BCIP/NBT staining, as shown in the pictures of the representative soft agar plates (right). The results are presented as percentages compared to the PBS-treated control. Error bars represent the mean ± s.d. ($n = 3$). $^{*}P < 0.05$, $^{**}P < 0.01$; n.s., not significant. The pictures are representative of three independent experiments.

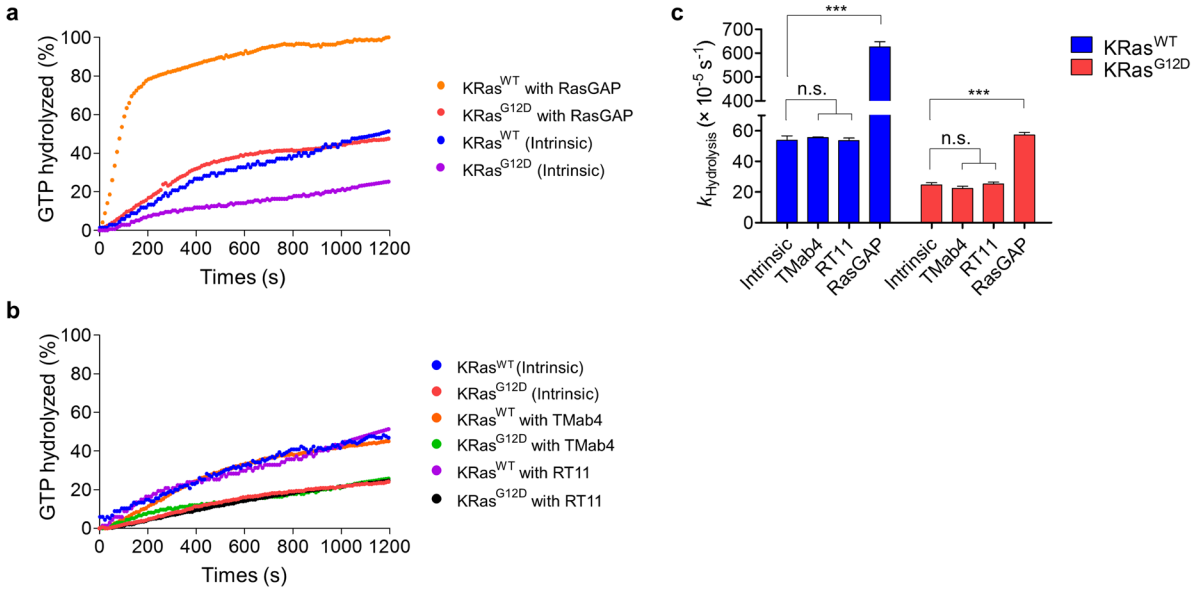


**Supplementary Figure 6 RT11 does not affect the intrinsic GTPase activity of KRas$^{WT}$ and KRas$^{G12D}$ proteins**. (**a**,**b**) Kinetic profiles of GTP hydrolysis of GTP-loaded KRas$^{WT}$ and KRas$^{G12D}$ proteins in the absence (intrinsic GTPase activity) and presence of GTPase-activating RasGAP protein (GAP-stimulated GTPase activity) (**a**) and the indicated antibodies (**b**). In (**a**), GAP-stimulated GTP hydrolysis was accessed with the catalytic domain of RasGAP (residues 714–1047)[7]. (**c**) Comparisons of GTP hydrolysis rate constants ($k$). GTP hydrolysis was determined by continuously measuring the release of phosphate using a purine nucleoside phosphorylase–based colorimetric assay[7]. The concentration of phosphate released *vs*. time was plotted and the first-order rate constant was determined. In (**c**), error bars represent the mean ± s.d. of three independent experiments. ***$P < 0.001$; n.s., not significant. The intrinsic and RasGAP-stimulated GTP hydrolysis rate constants of KRas$^{WT}$ and KRas$^{G12D}$ were comparable to those reported earlier[7].

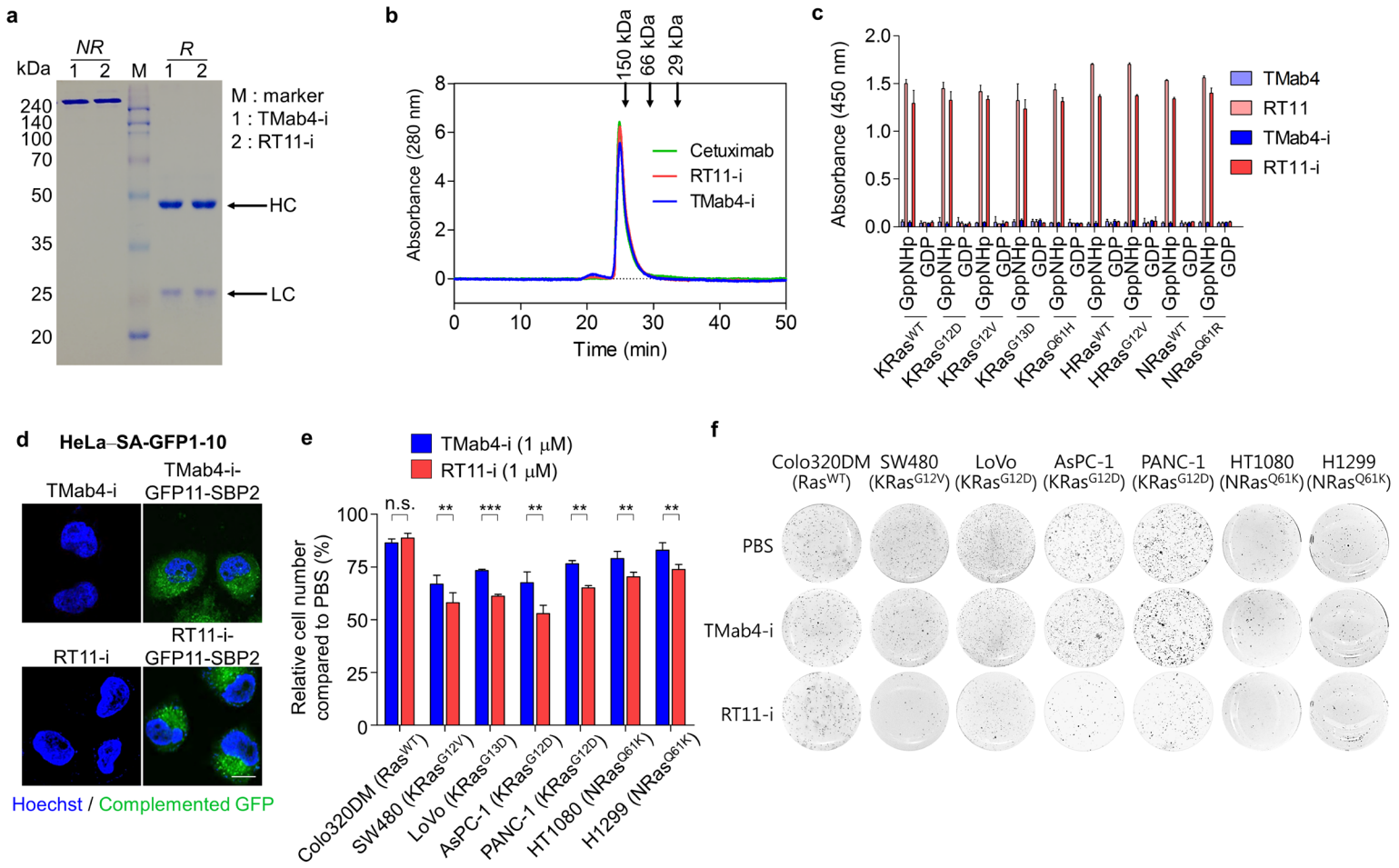


**Supplementary Figure 7 Biochemical and biological characterization of RGD10 peptide-fused RT11-i iMab.** (**a**) Reducing ('*R*') and non-reducing ('*NR*') SDS-PAGE analyses of the purified antibodies (each 5 μg) in the human IgG1 format. (**b**) Size exclusion elution profiles of purified TMab4-i and RT11-i (50 μl of 100 μg ml$^{-1}$) monitored at 280 nm. Cetuximab (50 μl of 100 μg ml$^{-1}$) was included as a control. The

arrows indicate the elution positions of molecular weight standards. Two independent analyses were performed with the same results. (**c**) ELISA showing the selective binding of RT11-i, but not TMab4-i, to GppNHp-bound active Ras variants over GDP-bound inactive forms at comparable levels to those observed with RT11. Error bars represent the mean ± s.d. ($n$ = 3). (**d**) Cellular internalization and cytosol localization of TMab4-i and RT11-i, assessed by confocal microscopy for complemented GFP signals (green) in HeLa-SA-GFP1-10 cells after treatment with 1 μM of TMab4-i-GFP11-SBP2 and RT11-i-GFP11-SBP2 for 6 h. Scale bar, 20 μm. Nuclei were counterstained with Hoechst 33342 (blue). Scale bar, 20 μm. (**e**) Cellular proliferation assay under monolayer culture conditions with the indicated cells, treated twice at 0 and 72 h with 1 μM of RT11-i or TMab4-i for 6 d. Error bars represent the mean ± s.d. ($n$ = 3). $^{**}P < 0.01$, $^{***}P < 0.001$; n.s., not significant. (**f**) Inhibition of soft agar colony formation by RT11-i compared to that with TMab4-i, as described in Fig. 4f. The pictures are representative of three independent experiments.

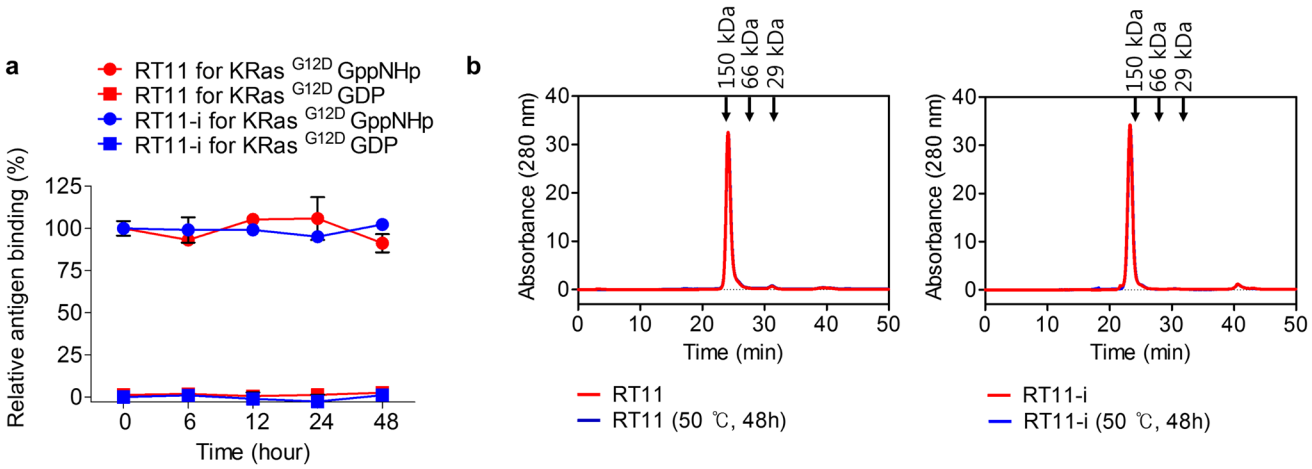


**Supplementary Figure 8 RT11-i possesses comparable thermal stability to that of RT11.** (**a**,**b**) Thermal stability of RT11 and RT11-i was assessed by ELISA for the selective antigen binding (**a**) and size exclusion chromatography (**b**) after incubating the antibodies (2 mg $ml^{-1}$) at 50 °C for the indicated periods. In (**a**), the binding activity (%) was relative to the initial binding of antibody stored at 4 °C. Error bars represent the mean ± s.d. ($n$ = 3). In (**b**), size exclusion chromatogram of antibodies (20 µl of 1 mg $ml^{-1}$) was monitored at 280 nm. Antibody stored at 4 °C was included as a control. Two independent analyses were performed with the same results. The arrows indicate the elution positions of molecular weight standards. SEC analysis of purified antibodies was performed on the Agilent 1100 high performance liquid chromatography system using a superdex$^{TM}$200 10/300GC (10 mm × 300 mm, GE Healthcare) size-exclusion column with a mobile phase of PBS buffer (pH 7.4) at a flow rate 0.5 ml $min^{-1}$.

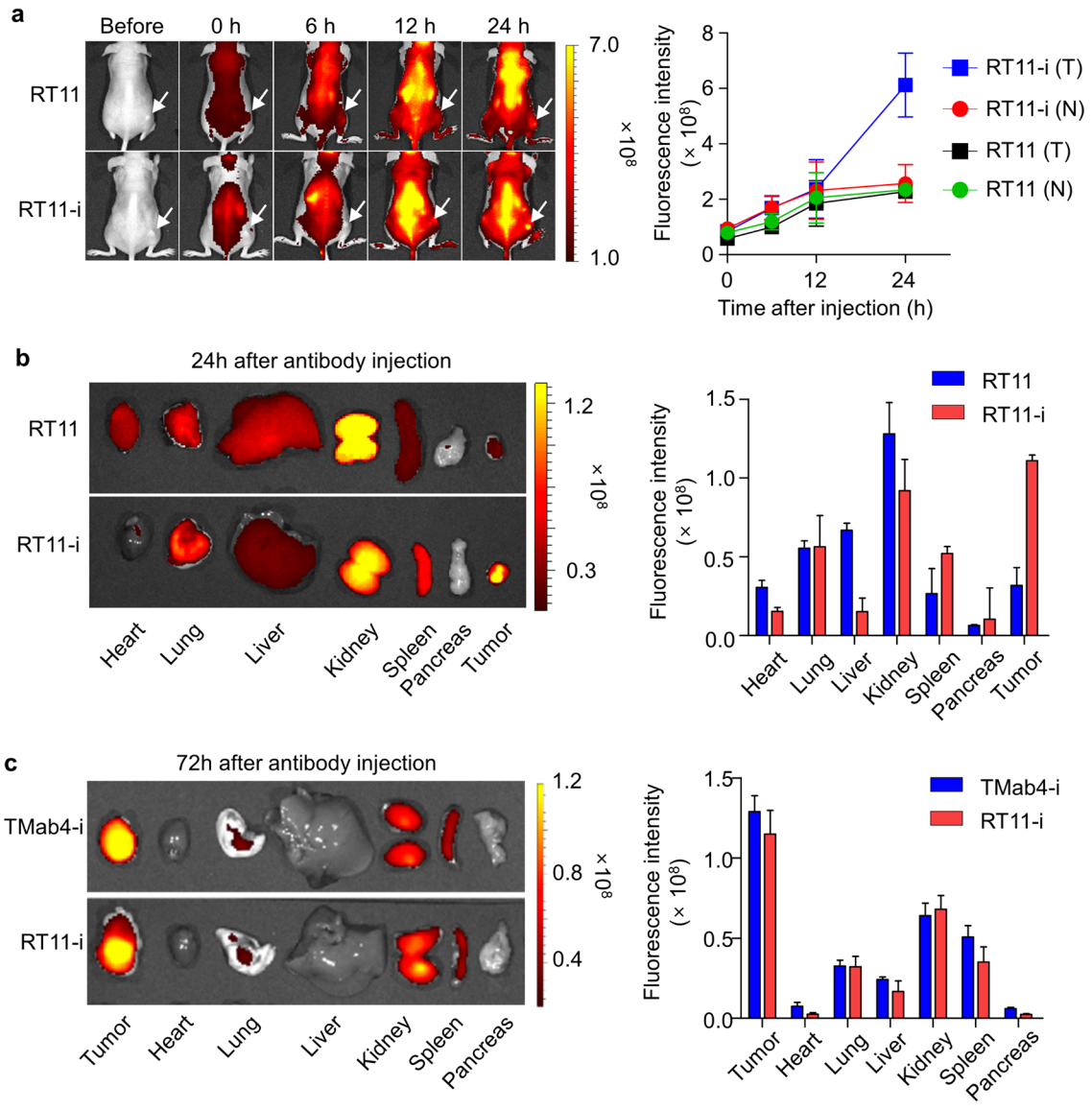
a
Before
0 h
6 h
12 h
24 h
RT11
RT11-i
7.0
1.0
× 10⁸
Fluorescence intensity (× 10⁸)
Time after injection (h)
RT11-i (T)
RT11-i (N)
RT11 (T)
RT11 (N)
b
24h after antibody injection
RT11
RT11-i
1.2
0.3
Heart
Lung
Liver
Kidney
Spleen
Pancreas
Tumor
c
72h after antibody injection
TMab4-i
RT11-i
1.2
0.8
0.4
Tumor
Heart
Lung
Liver
Kidney
Spleen
Pancreas

**Supplementary Figure 9 Preferential tumor tissue accumulation of TMab4-i and RT11-i in SW480 tumor-bearing xenograft mice. (a,b)** Comparison of biodistribution between RT11 and RT11-i, evaluated by intravenously injecting Dylight755-labeled antibodies (20 μg per mouse) into SW480 xenograft tumor-bearing mice. In (**a**), representative whole body fluorescence images, which were acquired at the indicated times post-injection. Fluorescence intensities in the tumor tissue (T), as indicated by arrows, and normal tissues (N) were quantified. In (**b**), *ex vivo* analysis of fluorescence intensities of dissected tumors and normal organs, which were acquired at 24 h post-injection. The right panel shows quantified fluorescence intensities of each tissue or organ. In (**a,b**), error bars represent the mean ± s.d. ($n$ = 6 per group). **(c)** *Ex vivo* analysis of fluorescence intensities for isolated tumors and normal organs 72 h after intravenous injection of Dylight755-labeled TMab4-i and RT11-i antibodies (20 μg per mouse) into mice bearing SW480 tumor xenografts, as shown in Fig. 5b. Error bars represent the mean ± s.d. ($n$ = 5 per group). In (**b,c**), tumor tissue and normal organs of one representative mouse from each group are shown. In (**a-c**), fluorescence intensities were quantified as radiant efficiency (photons $s^{-1}$ $cm^{-2}$ $steradian^{-1}$ per μW $cm^{-2}$) using Living Image software.

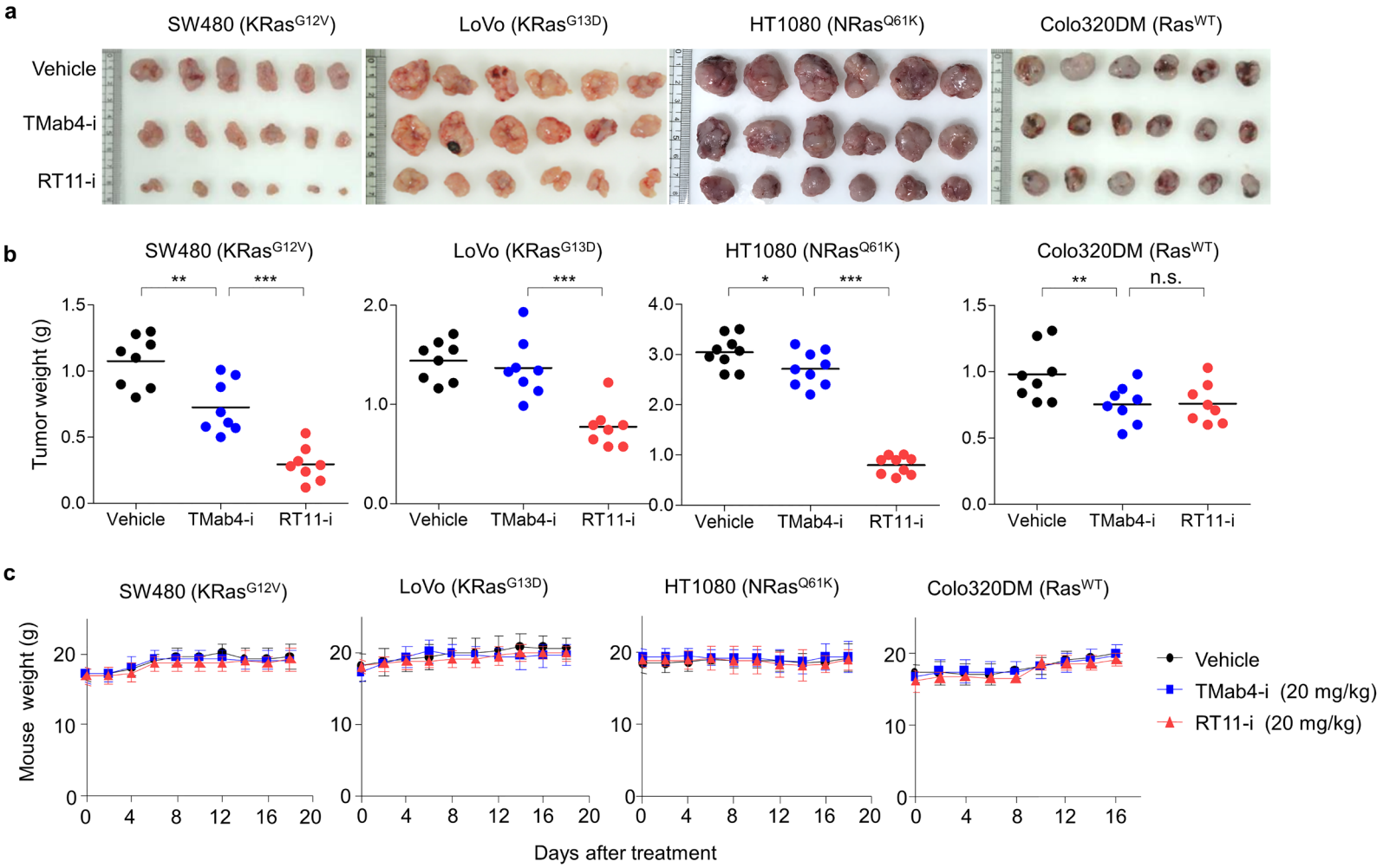
a
SW480 (KRas$^{G12V}$)
LoVo (KRas$^{G13D}$)
HT1080 (NRas$^{Q61K}$)
Colo320DM (Ras$^{WT}$)
Vehicle
TMab4-i
RT11-i
b
SW480 (KRas$^{G12V}$)
LoVo (KRas$^{G13D}$)
HT1080 (NRas$^{Q61K}$)
Colo320DM (Ras$^{WT}$)
Tumor weight (g)
**
***
*
n.s.
Vehicle
TMab4-i
RT11-i
c
SW480 (KRas$^{G12V}$)
LoVo (KRas$^{G13D}$)
HT1080 (NRas$^{Q61K}$)
Colo320DM (Ras$^{WT}$)
Mouse weight (g)
Days after treatment
Vehicle
TMab4-i (20 mg/kg)
RT11-i (20 mg/kg)

**Supplementary Figure 10 RT11-i suppresses the *in vivo* growth of oncogenic Ras mutant tumor xenografts in mice.** (**a**) Representative photographs of tumors excised from mice following treatment described in Fig. 6a. (**b**) The weight of individual tumors from each treatment group, as described in Fig. 6a. *$P < 0.05$, **$P < 0.01$, ***$P < 0.001$; n.s., not significant. (**c**) Mouse weight measured during the treatments described in Fig. 6a. Notably no signs of systemic toxicity (e.g., no significant changes in body weight, gross appearance, or behavior) were observed in mice treated with TMab4-i or RT11-i, compared to those in vehicle-treated mice. In (**b,c**), error bars represent the mean ± s.d. ($n$ = 8 per group).

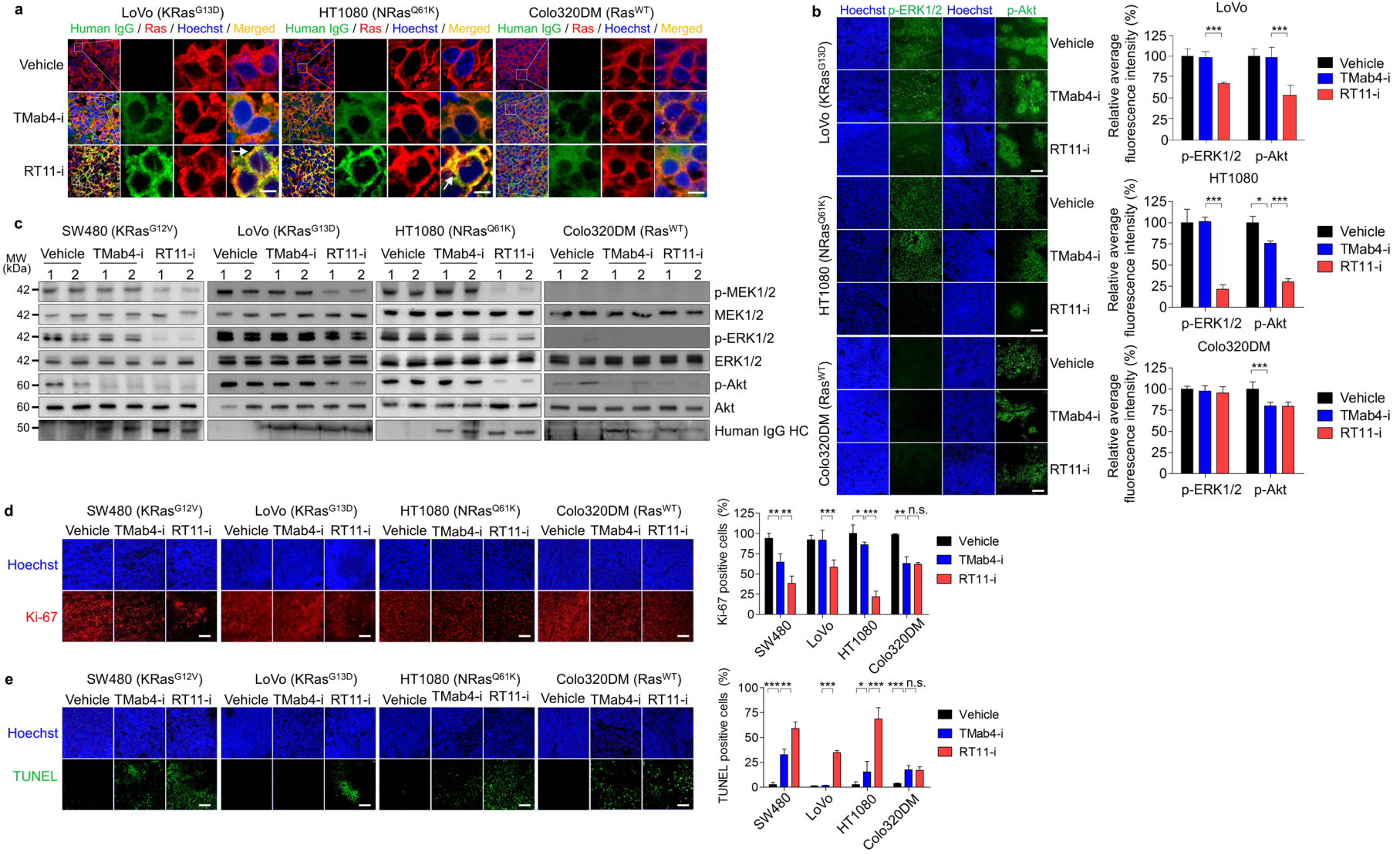
a
LoVo (KRasG13D)
HT1080 (NRasQ61K)
Colo320DM (RasWT)
Human IgG / Ras / Hoechst / Merged
Vehicle
TMab4-i
RT11-i
b
Hoechst p-ERK1/2 Hoechst p-Akt
LoVo (KRasG13D)
HT1080 (NRasQ61K)
Colo320DM (RasWT)
Relative average fluorescence intensity (%)
p-ERK1/2
p-Akt
c
SW480 (KRasG12V)
LoVo (KRasG13D)
HT1080 (NRasQ61K)
Colo320DM (RasWT)
MW (kDa)
p-MEK1/2
MEK1/2
p-ERK1/2
ERK1/2
p-Akt
Akt
Human IgG HC
d
Hoechst
Ki-67
Ki-67 positive cells (%)
n.s.
e
TUNEL
TUNEL positive cells (%)

**Supplementary Figure 11 Immunohistochemical and western blot analyses of tumor tissues excised from mice, as described in Fig 6a.** (**a**) Cellular penetration and co-localization of RT11-i (green), but not TMab4-i (green), with activated Ras (red) in oncogenic KRas mutant-harboring LoVo and NRas mutant-harboring HT1080 tumor tissues. In the $Ras^{WT}$-harboring Colo320DM tissues, both RT11-i (green) and TMab4-i (green) were internalized into cells, but did not significantly co-localize with $Ras^{WT}$ proteins, likely because the $Ras^{WT}$ proteins are not highly activated. Scale bar, 10 μm. (**b**) Analysis of p-ERK1/2 (green) and p-Akt (green) levels in LoVo, HT1080, and Colo320DM tumor tissues. Scale bar, 100 μm. The right panels show the percentage of relative fluorescence intensity compared to that in the vehicle-treated control. Error bars represent the mean ± s.d. of five random fields for each immunofluorescence sample (*n* = two tumors per group). (**c**) Western blot analysis of tumor tissue lysates prepared after treatment, as described in Fig. 6a to analyze the downstream signaling activation of Raf-MEK1/2-ERK1/2 and PI3K-Akt pathways. As indicated, two independent tumor tissue samples (sample 1 and sample 2) were analyzed. (**d,e**) Tumor cell proliferation and apoptosis were determined in tumor tissues through Ki-67 staining (**d**) and TUNEL staining (**e**), respectively. Scale bar, 100 μm. The right panels show the percentage of Ki-67-positive (**d**) and TUNEL-positive (**e**) cells compared to the number of Hoechst 33342-stained cells for each sample. Error bars represent the mean ± s.d. of five random fields for each immunofluorescence sample (*n* = two tumors per group). In (**a, b, d** and **e**), nuclei were counterstained with Hoechst 33342 (blue). In (**b,d** and **e**), statistical analyses were performed using a one-way ANOVA followed by the Newman-Keuls post-test. $*P < 0.05$, $**P < 0.01$, $***P < 0.001$ *vs*. TMab4-i; n.s., not significant. Images are representative of at least two independent experiments.

**Figure 2c**

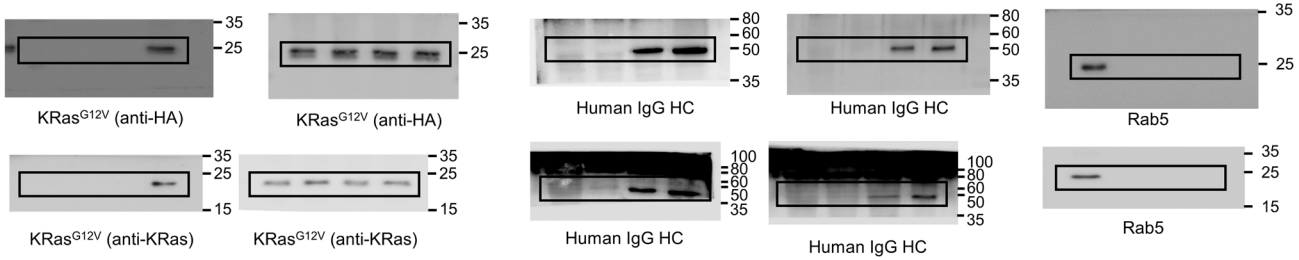


**Figure 3c**

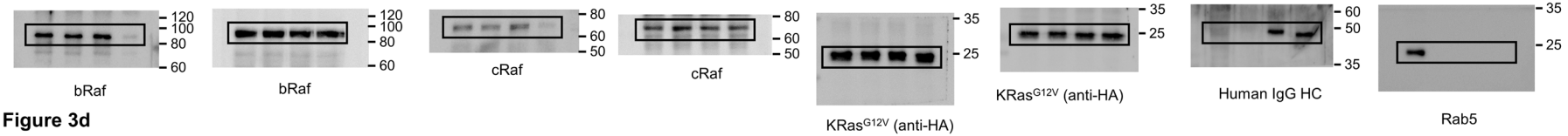


**Figure 3d**

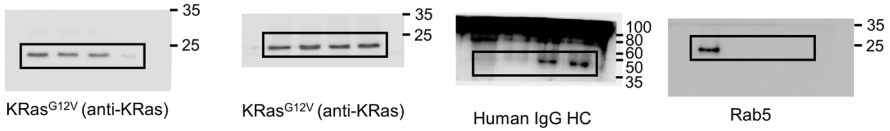


**Figure 3e**

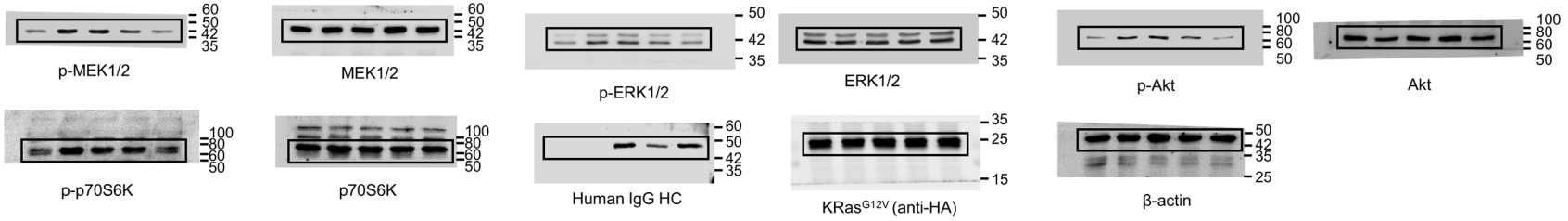


**Supplementary Figure 12 Unprocessed scans of western blots.**

**Figure 3f**

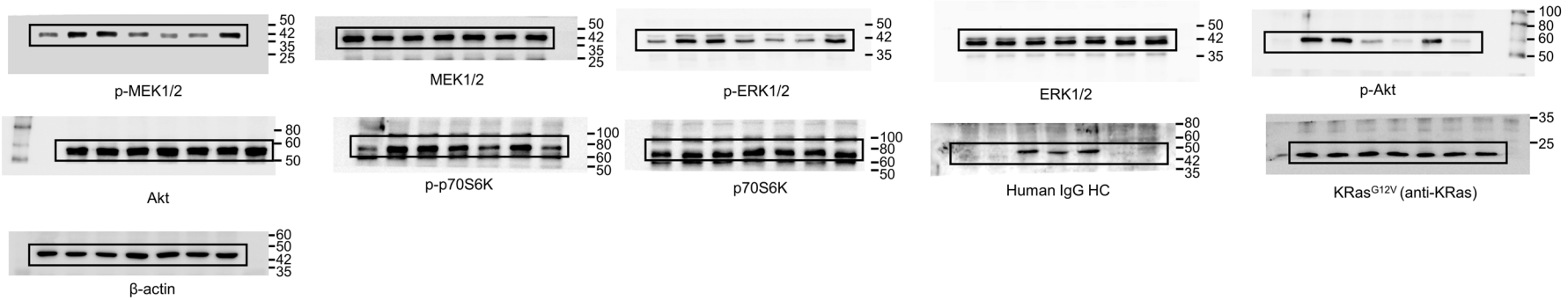


**Figure 4e**

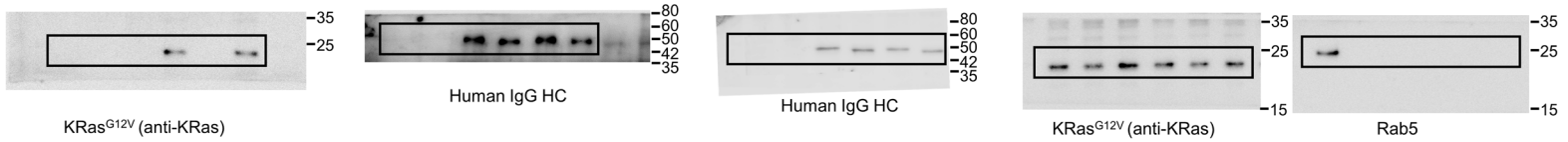


**Supplementary Figure 12 Unprocessed scans of western blots. (Continued)**

**Supplementary Table 1 Binding constants for the interactions of RT11 and RT11-i with GppNHp-loaded active forms of Ras, determined by SPR.**

| Anti-bodies | Ras proteins | Kinetic parameters [a] | | |
|---|---|---|---|---|
| | | $k_a$ ($M^{-1}s^{-1}$) | $k_d$ ($s^{-1}$) | $K_D$ (M) |
| RT11 | $KRas^{WT}$·GppNHp | $(2.77 \pm 0.72) \times 10^{5}$ | $(3.30 \pm 0.15) \times 10^{-3}$ | $(1.09 \pm 0.58) \times 10^{-8}$ |
| | $KRas^{G12D}$·GppNHp | $(8.04 \pm 2.51) \times 10^{4}$ | $(9.07 \pm 1.68) \times 10^{-4}$ | $(1.11 \pm 0.29) \times 10^{-8}$ |
| | $KRas^{G12V}$·GppNHp | $(9.11 \pm 1.17) \times 10^{4}$ | $(1.41 \pm 0.49) \times 10^{-3}$ | $(1.65 \pm 0.44) \times 10^{-8}$ |
| | $KRas^{G13D}$·GppNHp | $(1.27 \pm 0.31) \times 10^{5}$ | $(2.22 \pm 0.67) \times 10^{-3}$ | $(1.55 \pm 0.84) \times 10^{-8}$ |
| | $KRas^{Q61H}$·GppNHp | $(5.22 \pm 0.91) \times 10^{4}$ | $(7.44 \pm 0.84) \times 10^{-4}$ | $(1.58 \pm 0.51) \times 10^{-8}$ |
| | $HRas^{WT}$·GppNHp | $(6.46 \pm 0.75) \times 10^{5}$ | $(2.17 \pm 0.71) \times 10^{-3}$ | $(3.62 \pm 1.32) \times 10^{-9}$ |
| | $HRas^{G12V}$·GppNHp | $(2.55 \pm 1.02) \times 10^{5}$ | $(1.41 \pm 0.52) \times 10^{-3}$ | $(5.01 \pm 1.12) \times 10^{-9}$ |
| | $NRas^{WT}$·GppNHp | $(3.19 \pm 1.11) \times 10^{4}$ | $(3.55 \pm 0.48) \times 10^{-4}$ | $(1.14 \pm 0.44) \times 10^{-8}$ |
| | $NRas^{Q61R}$·GppNHp | $(3.31 \pm 0.66) \times 10^{4}$ | $(3.68 \pm 0.65) \times 10^{-4}$ | $(1.21 \pm 0.41) \times 10^{-8}$ |
| RT11-i | $KRas^{WT}$·GppNHp | $(1.65 \pm 0.24) \times 10^{5}$ | $(2.44 \pm 1.07) \times 10^{-3}$ | $(1.44 \pm 1.51) \times 10^{-8}$ |
| | $KRas^{G12D}$·GppNHp | $(3.33 \pm 0.55) \times 10^{4}$ | $(6.84 \pm 2.64) \times 10^{-4}$ | $(1.95 \pm 0.98) \times 10^{-8}$ |
| | $KRas^{G12V}$·GppNHp | $(5.42 \pm 2.10) \times 10^{4}$ | $(1.15 \pm 0.41) \times 10^{-3}$ | $(2.16 \pm 0.72) \times 10^{-8}$ |
| | $KRas^{G13D}$·GppNHp | $(8.01 \pm 1.72) \times 10^{4}$ | $(1.85 \pm 0.60) \times 10^{-3}$ | $(2.11 \pm 0.81) \times 10^{-8}$ |
| | $KRas^{Q61H}$·GppNHp | $(2.67 \pm 0.77) \times 10^{4}$ | $(4.95 \pm 0.44) \times 10^{-4}$ | $(1.95 \pm 0.88) \times 10^{-8}$ |
| | $HRas^{WT}$·GppNHp | $(4.41 \pm 1.60) \times 10^{5}$ | $(1.62 \pm 0.78) \times 10^{-3}$ | $(3.65 \pm 1.42) \times 10^{-9}$ |
| | $HRas^{G12V}$·GppNHp | $(2.36 \pm 0.88) \times 10^{5}$ | $(1.42 \pm 0.56) \times 10^{-3}$ | $(5.58 \pm 0.51) \times 10^{-9}$ |
| | $NRas^{WT}$·GppNHp | $(2.35 \pm 0.41) \times 10^{4}$ | $(2.91 \pm 0.88) \times 10^{-4}$ | $(1.11 \pm 0.89) \times 10^{-8}$ |
| | $NRas^{Q61R}$·GppNHp | $(2.09 \pm 0.42) \times 10^{4}$ | $(2.98 \pm 0.87) \times 10^{-4}$ | $(1.39 \pm 0.83) \times 10^{-8}$ |

[a] Each value represents the mean ± s.d. of two independent experiments. In each experiment, at least five data sets were used to determine the kinetic constants. The dissociation ($k_{off}$) and association rate constants ($k_{on}$), and the dissociation equilibrium constant ($K_D$) values, were determined by the 1:1 Langmuir binding model using the BIAevaluation software provided by the manufacturer.

**Supplementary Table 2 Quantitative assessment of cytosolic concentrations of RT11 and RT11-i in HeLa cells.**

| Parameters | Antibodies | Treated concentrations (μM) | | |
|---|---|---|---|---|
| | | **0.1** | **0.5** | **1** |
| Cytosolic amount (fmole)[a] | RT11 | 0.25 ± 0.12 | 1.51 ± 0.20 | 3.66 ± 0.20 |
| | RT11-i | 0.48 ± 0.03 | 2.41 ± 0.22 | 4.92 ± 0.29 |
| Cytosolic concentration (nM)[b] | RT11 | 14 ± 6 | 80 ± 11 | 195 ± 11 |
| | RT11-i | 25.3 ± 2 | 135 ± 12 | 308 ± 18 |

[a] The cytosolic amount was measured by enhanced split-GFP complementation assay obtained by incubation of HeLa-SA-GFP1-10 cells with RT11-GFP11-SBP2 and RT11-i-GFP11-SBP2 antibodies, as described in the Methods and in our previous work[8].

[b] The cytosolic molar concentration was estimated by dividing the cytosolic amount by the cytosolic volume of HeLa cells and cell numbers in each well, as described in the Methods and in our previous work[8].

## Supplementary Table 3 List of antibodies used in this study.

| Antibody | Applications | Company | Catalog no. | Dilution |
|---|---|---|---|---|
| c-myc | Flow cytometry | Ig therapy | A03002 | 1: 250 |
| Flag | Flow cytometry | Sigma-Aldrich | F3165 | 1: 250 |
| FITC-conjugated anti-human IgG (Fc specific) | Flow cytometry | Sigma-Aldrich | F9512 | 1 : 200 |
| Alexa Fluor 488-conjugated anti-mouse IgG | Flow cytometry | Invitrogen | A-11045 | 1 : 250 |
| PE-conjugated anti-human integrin αvβ3 | Flow cytometry | R&D systems, | FAB3050P, | 1:100 |
| PE-conjugated anti-human integrin αvβ5 | Flow cytometry | R&D systems, | FAB2528P | 1:100 |
| HRP-conjugated anti-GST | ELISA | Sigma-Aldrich | A7340 | 1 : 4000 |
| HRP-conjugated anti-His | ELISA | Sigma-Aldrich | A7058 | 1 : 2000 |
| Anti-human IgG (Fab specific) | ELISA | Sigma-Aldrich | I5260 | 1 : 400 |
| HRP-conjugated anti-human IgG | ELISA | Invitrogen | 62-8420 | 1 : 8000 |
| MEK1/2 | Western blot | Cell signaling | 9122 | 1 : 1000 |
| phospho-MEK1/2 | Western blot | Cell signaling | 9121 | 1 : 1000 |
| ERK1/2 | Western blot | Cell signaling | 4695 | 1 : 1000 |
| phospho-ERK1/2 | Western blot | Cell signaling | 4377 | 1 : 1000 |
| Akt | Western blot | Cell signaling | 9272 | 1 : 1000 |
| phospho-Akt | Western blot | Cell signaling | 9271 | 1 : 1000 |
| p70S6K | Western blot | Cell signaling | 9202 | 1 : 1000 |
| phospho-p70S6K | Western blot | Cell signaling | 9205 | 1 : 1000 |
| Rab5 | Western blot | Cell signaling | 3547 | 1 : 1000 |
| HA | Western blot | Covance | MMS-101P | 1 : 1000 |
| KRas | Western blot | Santa Cruz | sc-30 | 1 : 500 |
| bRaf | Western blot | Santa Cruz | sc-5284 | 1 : 500 |
| cRaf | Western blot | Santa Cruz | sc-133 | 1 : 500 |
| β-actin | Western blot | Santa Cruz | sc-69879 | 1 : 1000 |
| HRP-conjugated anti-mouse IgG | Western blot | Santa Cruz | sc-2031 | 1 : 4000 |
| HRP-conjugated anti-rabbit IgG | Western blot | Santa Cruz | sc-2004 | 1 : 4000 |
| HRP-conjugated anti-goat IgG | Western blot | Santa Cruz | sc-2033 | 1 : 4000 |
| Anti-human IgG (Fc specific) | Western blot | Invitrogen | 31125 | 1 : 1000 |
| Ras | Immunofluorescence Immunohistochemistry | Abcam | ab108602 | 1 : 100 |
| Alexa Fluor 488-conjugated anti-human IgG | Immunofluorescence Immunohistochemistry | Invitrogen | A-11013 | 1 : 500 |
| TRITC-conjugated anti-rabbit IgG | Immunofluorescence Immunohistochemistry | Sigma-Aldrich | T6778 | 1 : 250 |
| phospho-ERK1/2 | Immunohistochemistry | Abcam | ab9272 | 1 : 100 |
| Ki-67 | Immunohistochemistry | Abcam | ab15580 | 1 : 100 |
| phospho-Akt | Immunohistochemistry | Cell signaling | 9271 | 1 : 100 |
| phospho-STAT3 (T705) | Immunohistochemistry | Cell signaling | 9145 | 1 : 100 |
| phospho-STAT3 (S727) | Immunohistochemistry | Cell signaling | 9134 | 1 : 100 |
| FITC-conjugated anti-rabbit IgG | Immunohistochemistry | Chemicon | AP132F | 1 : 250 |

## Supplementary References


1. Sun, Q. *et al.* Discovery of small molecules that bind to K-Ras and inhibit Sos-mediated activation. *Angew. Chem. Int. Ed. Engl.* **51**, 6140-6143 (2012).
2. Scheidig, A. J., Burmester, C. & Goody, R. S. The pre-hydrolysis state of p21(ras) in complex with GTP: new insights into the role of water molecules in the GTP hydrolysis reaction of ras-like proteins. *Structure* **7**, 1311-1324 (1999).
3. Ye, M. *et al.* Crystal structure of M-Ras reveals a GTP-bound "off" state conformation of Ras family small GTPases. *J. Biol. Chem.* **280**, 31267-31275 (2005).
4. Cash, J. N., Davis, E. M. & Tesmer, J. J. Structural and Biochemical Characterization of the Catalytic Core of the Metastatic Factor P-Rex1 and Its Regulation by PtdIns(3,4,5)P3. *Structure* **24**, 730-740 (2016).
5. Karnoub, A. E. & Weinberg, R. A. Ras oncogenes: split personalities. *Nat. Rev. Mol. Cell Biol.* **9**, 517-531 (2008).
6. Matsumoto, K. *et al.* Critical roles of interactions among switch I-preceding residues and between switch II and its neighboring alpha-helix in conformational dynamics of the GTP-bound Ras family small GTPases. *J. Biol. Chem.* **286**, 15403-15412 (2011).
7. Hunter, J. C., Manandhar, A., Carrasco, M. A., Gurbani, D., Gondi, S. & Westover, K. D. Biochemical and Structural Analysis of Common Cancer-Associated KRAS Mutations. *Mol. Cancer Res.* **13**, 1325-1335 (2015).
8. Kim, J. S. *et al.* Quantitative assessment of cellular uptake and cytosolic access of antibody in living cells by an enhanced split GFP complementation assay. *Biochem. Biophys. Res. Commun.* **467**, 771-777 (2015).